International Journal of Multiphase Flow 36 (2010) 364–374

Contents lists available at ScienceDirect

International Journal of Multiphase Flow

journal homepage: www.elsevier.com/locate/ijmulflow

Multiscale simulation of flow and heat transfer of nanofluid with lattice Boltzmann method

Lujun Zhou, Yimin Xuan *, Qiang Li

School of Power Engineering, Nanjing University of Science & Technology, Nanjing 210094, China

ARTICLE INFO

Article history:
Received 11 August 2009
Received in revised form 9 January 2010
Accepted 9 January 2010
Available online 28 January 2010

Keywords:
Lattice Boltzmann method
Multiscale simulation
Nanofluid
Multicomponent flow

ABSTRACT

Based on the lattice Boltzmann (LB) approach, a novel hybrid method has been proposed for getting insight into the microscale characteristics of the multicomponent flow of nanofluid. In this method, the whole computational domain is divided into two regions in which different-sized meshes are involved for simulation (fine mesh and coarse mesh). The multicomponent LB method is adopted in the fine mesh region, and the single-component LB approach is applied to the coarse mesh region where the nanofluid is treated as a mixed single-component fluid. The conservation principles of mass, momentum and energy are used to derive a hybrid scheme across the different scaled regions. Numerical simulation is carried out for the Couette flow and convective heat transfer in a parallel plate channel to validate the hybrid method. The computational results indicate that by means of the present method, not only the microscopic characteristics of the nanofluid flow can be simulated, but also the computational efficiency can be remarkably improved compared with the pure multicomponent LB method.

1. Introduction

In 1995, Argonne proposed a new concept of so-called *nanofluids* which is a type of heat transfer fluids engineered by suspending ultrafine metallic or nonmetallic particles of nanometer dimensions in some base fluids (Choi, 1995). Generally, the nanofluids have some important characteristics: (1) they show significant enhancement in thermal conductivity (Kim et al., 2001), (2) they have more stable suspensibility compared with those fluids containing micro- and mini-scale particles (Lee et al., 1999) and (3) reduced chances of erosion because of these small momentum impart to a solid wall. In the recent years, the flow and heat transfer features of the nanofluids have been widely investigated by means of both experimental and theoretical approaches (Lee et al., 1999; Wang et al., 1999; Arulmurugan et al., 2005; Xuan and Li, 2000; Das et al., 2003, 2006; Enomoto et al., 2003).

As shown in Fig. 1, the nanofluid is a typical example that one may find different understandings on fluid morphology, flow and thermal processes if different scales are involved. At the macroscopic level, the nanofluid may be assumed to be an even-mingled fluid with single-phase features. At the microscopic level, the nanofluid is a two-phase fluid whose multicomponent features cannot be neglected. Since the diameter of suspended particles are at the level of nanometer, it is still a tough work to get fine insight into the flow and energy transport processes of nanofluids at the microscale with the conventional numerical approach. If one tries to get microscopic view on the flow and thermal processes of nanofluids, the computational grids must be ultrafine to deliver information about the multicomponent features of nanofluids at the microscale and the computation cost may not be bearable for a real flow in a channel. On the other hand, the assumption of considering the nanofluid as a single-component fluid may be acceptable and it may not be necessary to handle the nanofluid as a two-component medium in most regions of the channel except the interesting area such as the regions near the channel wall. Thus, a multiscale algorithm may be desirable and feasible for one to investigate the complicated flow and heat transfer processes of the nanofluid, which combines the multicomponent model and the single component model.

As an effective numerical approach, the lattice Boltzmann method (LBM) based on microscopic model and mesoscopic kinetic equation appeared in the 1980s (McNamara and Zanetti, 1988; Higuera et al., 1989; Higuere and Jimenez, 1989). The obvious advantages of LBM are the simplicity of programming, the parallelism of the algorithm and the capability of incorporating complex microscopic interactions. This method has been demonstrated its ability to simulate single component hydrodynamics, multiphase and multicomponent fluids (Shan and Chen, 1993; Swift et al., 1996; Sofonea and Frueh 2001; Love et al., 2003), thermal convection (Massaioli, 1993), flows through porous media (Pan et al., 2004; Ahrenholz et al., 2006), magnetohydrodynamic (Dellar, 2002), and compressible flow (Li et al., 2007) and so on. To extend the standard LBM to complex physical phenomena which may be

* Corresponding author. Tel.: +86 25 8431 5700; fax: +86 25 8443 1339.
E-mail address: ymxuan@mail.njust.edu.cn (Y. Xuan).

0301-9322/$ - see front matter © 2010 Elsevier Ltd. All rights reserved.
doi:10.1016/j.ijmultiphaseflow.2010.01.005

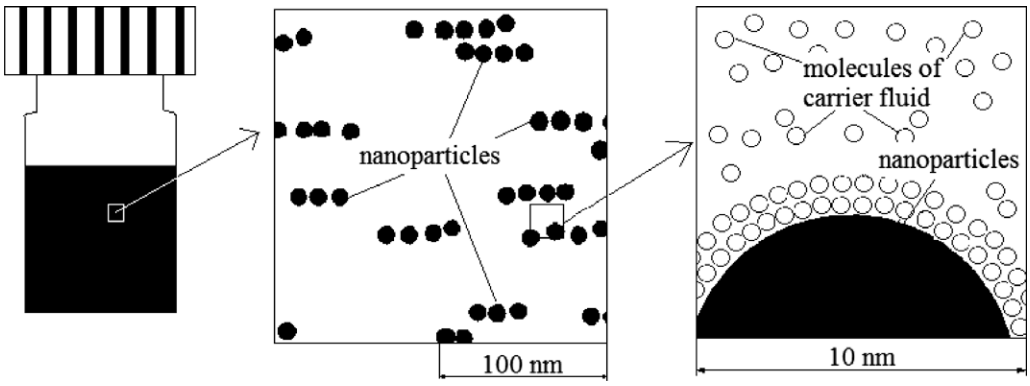

Fig. 1. Schematic of nanofluid on different scale.

across different length and time scales, researchers have attempted to use irregular lattices and proposed several novel models (Hortmann et al., 1990; Nannelli and Succi, 1992; He et al., 1996; Cao et al., 1997; Filippova and Haenel, 1998; Kandhai et al., 2000; Shu et al., 2001; Yu et al., 2002; Dupuis and Chopard, 2003; Ubertini et al., 2003; Li et al., 2004; Stiebler et al., 2006; Chen et al., 2006; Kwon and Hosoglu, 2008; Patil and Lakshmisha, 2009). Generally, the irregular lattices methods can be separated into two categories (as shown in Fig. 2): one is based on the spatial interpolation in which the grids are irregular in the total computational areas and the physical parameters on the grids are achieved by interpolation (Cao et al., 1997; Stiebler et al., 2006). Some researchers used the locally embedded grid approach that the computational area is segmented into different regions with different-sized uniform grid, where the physical information is exchanged by a coupling boundary (such as Filippova and Haenel, 1998; Yu et al., 2002). However, the above mentioned irregular lattices approaches are applied to single component flow only, which may be difficult to be used for simulating multicomponent flow straightly.

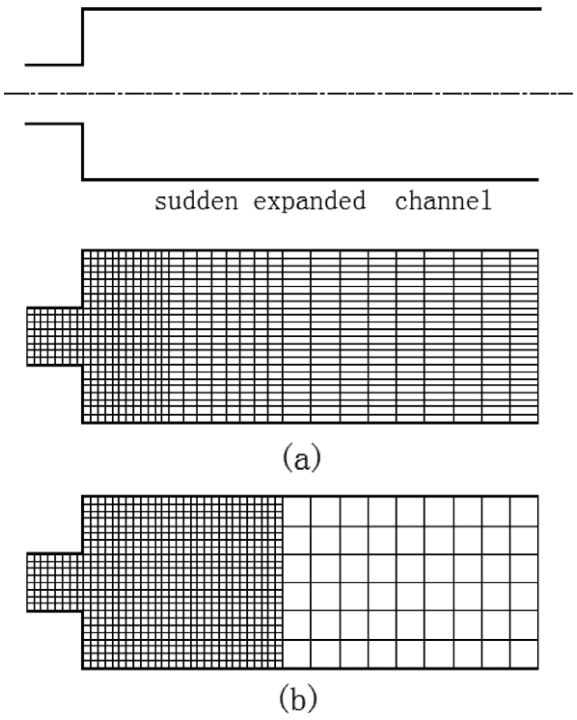

Fig. 2. Schematic nonuniform grids: (a) unstructured grids and (b) locally embedded grids.

In this paper, we apply the multiscale analysis approach to simulating flow and thermal processes of the nanofluid based on the lattice Boltzmann method. As shown in Fig. 1, on the mesoscale the nanofluid is regarded as a binary component fluid, and that the suspended nanoparticles phase and the base fluid phase should be handled separately, but at the macroscale the nanoparticles and the base fluid are incorporated into a mixer and the nanofluid can be regarded as single component one. We use a novel hybrid method of multicomponent and single-component hybrid method (MSHM) for studying flow and thermal processes of the nanofluid. In the present method, the computational domain is divided into two regions with different-sized uniform grids (fine mesh and coarse mesh). On the fine meshes the multicomponent lattice Boltzmann model (MLBM) is used to investigate the binary component features of the nanofluid and the single-component lattice Boltzmann model (SLBM) is adopted on the coarse meshes to reduce the computational time. In order to ensure the continuity of the physical information (physical parameters) in the hybrid region, the principles of mass and momentum conservations are obeyed. Examples of Couette flow and heat transfer process are introduced to validate the feasibility of the MSHM. The flow and heat transfer characteristics of the nanofluid are investigated. In addition, the relationship between the computational capability of MSHM and the refinement parameter n as well as the area ratio Φ is discussed (Φ is the ratio of the volume treated with multicomponent method to the total volume). The paper is organized in the following: Firstly, the multicomponent and single-component hybrid methods are described in Section 2 and more attention is paid to explain the algorithm of handling transfer of physical variables across the boundary between two different scaled regions. Then two examples are introduced to validate the accuracy of the present hybrid method in Section 3. Finally, the computation efficiency of the hybrid method is discussed.

2. Multicomponent and single-component hybrid method (MSHM)

The grid schematic of the MSHM is shown in Fig. 3. The coarse mesh region and the fine mesh region are overlapped and a hybrid region is formed. The shadows around point C and F represent the coarse grid area and fine grid area, respectively. To make description clear, some terms are first explained here. Coarse mesh boundary refers to the boundary of the coarse mesh region that lies in the fine mesh area. For example, point C in Fig. 3 belongs to the coarse mesh boundary. Similarly, fine mesh boundary indicates the boundary of fine mesh region that drops in the coarse mesh region and typical examples are points A, B and G as shown in Fig. 3. Hybrid region is for the region between fine mesh boundary and

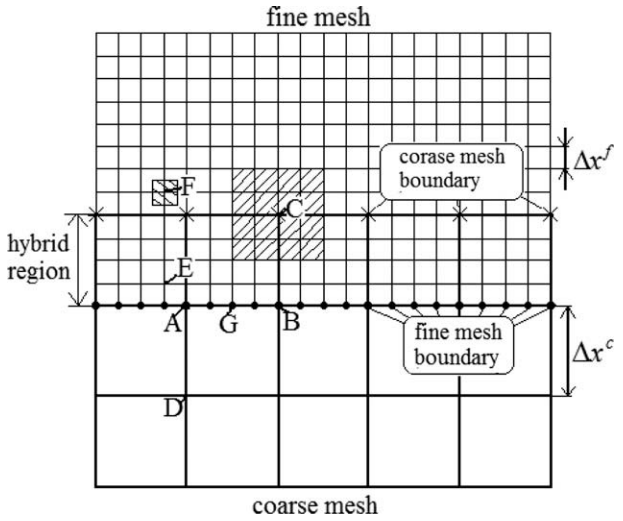

Fig. 3. Interface of coarse mesh and fine mesh at a parameter of refinement 4.

coarse mesh boundary. The crossing and circle points represent the coarse mesh boundary sites and fine mesh boundary sites, respectively.

On the assumption that the speed of sound is constant on different meshes, one has:

$$\frac{\Delta x^c}{\Delta t^c} = \frac{\Delta x^f}{\Delta t^f} \tag{1}$$

where the superscripts f and c respectively stand for the fine mesh and coarse mesh. Δx and Δt represent the spatial step and time step, respectively.

For the sake of convenience of numerical computation, the wrapped trick for coupling the numerical procedures between the coarse and fine regions is used without loss of generality. For such a purpose, one can select the refinement parameter n as (Filippova and Haenel, 1998):

$$\frac{\Delta x^c}{\Delta x^f} = \frac{\Delta t^c}{\Delta t^f} = n \tag{2}$$

Obviously, the value of this refinement parameter n dominates the computational efficiency and it will be investigated in the following context. To keep the same viscosity on the coarse grids and fine grids, the relaxation time parameter on the fine mesh region comply with the following relationship:

$$\tau^f = \frac{1}{2} + n\left(\tau^c - \frac{1}{2}\right) \tag{3}$$

where τ^f and τ^c stand for the relaxation time on fine mesh and coarse mesh of the mixed fluid, respectively.

In this section, we first introduce the SLBM which is applied in the coarse mesh region, and then the MLBM is for the fine mesh region to deliver the two-component feature of nanofluids. Special attention is paid to the overlapped region of coupling the two regions with different scales. With the method being similar to those used by Shan (1997) and Guo et al. (2002a), the Double Distribution Function (DDF) model is introduced to describe the momentum and energy transport processes corresponding to both SLBM and the MLBM.

2.1. Single-component lattice Boltzmann model

According to the well-known D2Q9 model of LBM, the evolution equations of the velocity and temperature for the single-phase nanofluid are:

$$f_i(\mathbf{x} + \Delta t^c \mathbf{c}_i, t + \Delta t^c) - f_i(\mathbf{x}, t) = -\frac{1}{\tau}\left(f_i(\mathbf{x}, t) - f_i^{eq}(\mathbf{x}, t)\right) \tag{4}$$

$$g_i(\mathbf{x} + \Delta t^c \mathbf{c}_i, t + \Delta t) - g_i(\mathbf{x}, t) = -\frac{1}{\tau_T}\left(g_i(\mathbf{x}, t) - g_i^{eq}(\mathbf{x}, t)\right) \tag{5}$$

where τ and τ_T respectively are the relaxation-time factor for the relevant collision process of particles, $\mathbf{c}_i$ is the discrete velocity vector, and f_i^{eq} and g_i^{eq} are the velocity and temperature equilibrium distribution functions which are given as follows:

$$f_i^{eq} = \rho\omega_i\left(1 + \frac{\mathbf{u}^{eq}\cdot\mathbf{c}_i}{c_s^2} + \frac{(\mathbf{u}^{eq}\cdot\mathbf{c}_i)^2}{2c_s^4} - \frac{\mathbf{u}^{eq2}}{2c_s^2}\right) \tag{6}$$

$$g_i^{eq} = \frac{T}{4}\left(1 + 2\frac{\mathbf{c}_i\cdot\mathbf{u}^{eq}}{c^2}\right) \tag{7}$$

where ρ, $\mathbf{u}^{eq}$ and T represent the density, the flow velocity and temperature of the nanofluid, respectively. Parameter ω_i is the weight coefficients.

$$\omega_i = \begin{cases} \frac{4}{9} & i = 0 \\ \frac{1}{9} & i = 1,\ldots,4 \\ \frac{1}{36} & i = 5,\ldots,8 \end{cases} \tag{8}$$

The macroscopic variables ρ, $\mathbf{u}^{eq}$, and T are the lattice variables comply with the following relationships:

$$\rho = \sum_{i=0}^{8} f_i \tag{9}$$

$$\rho\mathbf{u}^{eq} = \sum_{i=0}^{8} \mathbf{c}_i f_i \tag{10}$$

$$T = \sum_{i=1}^{4} g_i \tag{11}$$

2.2. Multicomponent lattice Boltzmann model

It is well known that the lattice Boltzmann equation originates from the microscopic understanding of physical phenomena by means of the distribution and momentum of the fictitious particles. The two-component lattice Boltzmann method assumes that the nanoparticles are mesoscopically located at a series of lattices and the particles distribution can be expressed as $f(\mathbf{x}, \mathbf{v}, t)$ (Xuan and Yao, 2005). Even this algorithm cannot get the tracks of single particles, but it can significantly reduce the computation time with accounting for the complicated forces involved in the nanofluid ensemble. Here the algorithm of two-component lattice Boltzmann method established in the previous work (Xuan and Yao, 2005) is extended to multiscale algorithm for simulating the nanofluid, in which the two-component lattice Boltzmann approach is mainly applied to the fine mesh region. The evolution equations of the velocity and temperature are written for each component α in the nanofluid (Shan and Chen, 1993):

$$f_i^{\alpha}(\mathbf{x} + \Delta t^f \mathbf{c}_i, t + \Delta t) - f_i^{\alpha}(\mathbf{x}, t) = -\frac{1}{\tau^{\alpha}}\left(f_i^{\alpha}(\mathbf{x}, t) - f_i^{\alpha,eq}(\mathbf{x}, t)\right) \tag{12}$$

$$g_i^{\alpha}(\mathbf{x} + \Delta t^f \mathbf{c}_i, t + \Delta t) - g_i^{\alpha}(\mathbf{x}, t) = -\frac{1}{\tau_T^{\alpha}}\left(g_i^{\alpha}(\mathbf{x}, t) - g_i^{\alpha,eq}(\mathbf{x}, t)\right) \tag{13}$$

where $f_i^{\alpha,eq}$ and $g_i^{\alpha,eq}$ are the velocity and temperature equilibrium distribution functions of the α component and they take the following forms:

$$f_i^{\alpha,eq} = \rho^{\alpha}\omega_i\left(1 + \frac{\mathbf{u}^{\alpha,eq}\cdot\mathbf{c}_i}{c_s^2} + \frac{(\mathbf{u}^{\alpha,eq}\cdot\mathbf{c}_i)^2}{2c_s^4} - \frac{\mathbf{u}^{\alpha,eq,2}}{2c_s^2}\right) \tag{14}$$

$$g_i^{\alpha,eq} = \frac{T}{4}\left(1 + 2\frac{\mathbf{c}_i \cdot \mathbf{u}^{\alpha,eq}}{c^2}\right) \tag{15}$$

where ρ^α and $\mathbf{u}^{\alpha,eq}$ present the lattice density and the velocity of component α of the nanofluid, respectively.

In the case that no internal and/or external forces and potentials act on the particles the total momentum of the particles of all components should be conserved by the collision term (Shan and Doolen, 1995). Thus, the equilibrium velocity $\mathbf{u}^{\alpha,eq}$ of each phase is equal to the mixed velocity of the two-component nanofluid as follows:

$$\mathbf{u}^{eq} = \frac{\sum_\alpha \rho^\alpha \mathbf{u}^\alpha/\tau^\alpha}{\sum_\alpha \rho^\alpha/\tau^\alpha} \tag{16}$$

Similarly, the averaged temperature of the nanofluid in the fine mesh region yields

$$T = \frac{\sum_\alpha \rho^\alpha c_p^\alpha T^\alpha/\tau_T^\alpha}{\sum_\alpha \rho^\alpha c_p^\alpha/\tau_T^\alpha} \tag{17}$$

where c_p^α is the specific heat capacity of component α.

Expression (16) is for the case that neither internal nor external forces and/or potentials act on the lattice particles. Any possible force sum $\mathbf{F}^\alpha$ acting on component α will result in momentum variation $\mathbf{F}^\alpha\tau^\alpha\Delta t$. In the presence of force vector sum $\mathbf{F}^\alpha$, the equilibrium velocity of component α is modified by

$$\rho^\alpha \mathbf{u}^{\alpha,eq} = \rho^\alpha \mathbf{u}^{eq} + \mathbf{F}^\alpha \tau^\alpha \Delta t \tag{18}$$

It is clear that the equilibrium velocity $\mathbf{u}^{\alpha,eq}$ may be different from component to component because the force vector $\mathbf{F}^\alpha$ may be different for each component, which is important for the fine mesh region. This expression reminds us of the fact that there exists the velocity slip between the suspended nanoparticles component and the ambient carrier liquid at the mesoscopic level.

Similarly, by taking the energy exchange between the nanoparticles component and the ambient fluid in the fine region into account, the equilibrium temperature of component α is modified as (Xuan et al., 2006):

$$T^{\alpha,eq} = T^\alpha + \Delta t\frac{dT}{dt} = T^{\alpha,eq} + \Delta t\varphi_{\alpha\bar{\alpha}} \tag{19}$$

where $\varphi_{\alpha\bar{\alpha}} = \frac{h_{\alpha\bar{\alpha}}[T^{\bar{\alpha}}(x,t-\Delta t) - T^\alpha(x,t-\Delta t)]}{\rho^\alpha c_p^\alpha a^\alpha}$, and $h_{\alpha\bar{\alpha}}$ is the convective heat transfer coefficient of nanofluid.

By summing the velocities for both components, we get the velocity of the mixed fluid:

$$\bar{\mathbf{u}} = \left(\sum_\alpha \rho^\alpha \mathbf{u}^\alpha + \frac{\Delta t}{2}\sum_\alpha F^\alpha\right) \Big/ \sum_\alpha \rho^\alpha \tag{20}$$

Thereafter, one can find the slip velocity of each component with mixed fluid as:

$$\Delta\mathbf{u}^\alpha = \mathbf{u}^{\alpha,eq} - \bar{\mathbf{u}} \tag{21}$$

The slip velocity describes the velocity difference between equilibrium velocity of component α and the mixed velocity $\bar{\mathbf{u}}$, which will be used in the coupling process.

2.3. Coupling in hybrid region of MSHM

The major difficulty of multiscale simulation for a fluid system lies in coupling the all variables and parameters descriptions from different scale regions. Since the multiscale descriptions are artificially introduced, the variables and parameters should be kept to be physically continuous at the artificial interface between two adjacent regions with different scales. Therefore, a suitable coupling scheme is vital for any multiscale method. Establishing an overlap region is a common approach for multiscale simulation, which plays a role of buffer to avoid sharp oscillations of variables and parameters such as velocity and temperature at the interface and allow the variable solutions from the different scaled regions to relax and to be coupled together (Nie et al., 2004).

As shown in Fig. 3, a hybrid or overlap region is constructed between the coarse and fine mesh regions. The physical variables of the nanofluid on the coarse mesh boundary are obtained by means of integration of the same variables from the fine grids. On the other hand, the physical variables of each component of the nanofluid on the fine mesh boundary are obtained by interpolation from the coarse grids. The processes of transformation from f_i^f to f_i^c (or from f_i^c to f_i^f) on the hybrid region are divided into three steps. Firstly, by integrating process of $f_i^f, c_i f_i^f, g_i^f$, (or $f_i^c, c_i f_i^c, g_i^c$) we can get the physical parameters of density, velocity and temperature on the fine mesh region (or coarse mesh region). Then, by integration of these physical variables of nanofluid on the corresponding fine grids (or by interpolation of physical variables on the coarse grids), the physical variables on the coarse (or fine) mesh boundary are obtained. Finally, by means of the non-equilibrium extrapolation method (Guo et al., 2002b), the distributions of f_i^c (or f_i^f) on the boundary can be obtained. The detailed processes are described in the following.

2.3.1. Coupling transition from the fine mesh region to the coarse mesh region

The purpose of coupling transition from the fine region to the coarse region is to derive the boundary information for the numerical simulation of SLBM on coarse mesh region. As shown in Fig. 3, integrating or summing the variables and parameter such as the density, velocity, and temperature for both components along the fine grids will provide the relevant averaged values for the coarse region. With regards to the continuum and conservation features of the incompressible nanofluid flow, we have:

$$\rho V^c = \sum_{V^f}\sum_\alpha \rho^\alpha V^f \tag{22}$$

$$\rho \mathbf{u} V^c = \sum_{V^f}\sum_\alpha \rho^\alpha \mathbf{u}^\alpha V^f \tag{23}$$

$$\rho c_p T V^c = \sum_{V^f}\sum_\alpha \rho^\alpha c_p^\alpha T^\alpha V^f \tag{24}$$

$$\mathbf{F}^o V^c = \sum_{V^f}\sum_\alpha \mathbf{F}^\alpha V^f \tag{25}$$

where V^c is the volume of a single coarse grid, V^f is the volume of a single fine grid, $\mathbf{F}^o$ is the vector sum of all forces acting on the fluid, and $\mathbf{F}^\alpha$ is the vector sum of the internal and/or external forces on component α in the fine mesh region. By integrating these expressions, the relevant physical parameters have been obtained and then the post-collision distribution functions of the velocity and temperature on the boundary of coarse grids can be calculated by the non-equilibrium extrapolation scheme (Guo et al., 2002b):

$$f_i^c(\mathbf{x},t) = f_i^{c,eq}(\mathbf{x},t) + f_i^{c,neq}(\mathbf{x}_a,t) \tag{26}$$

$$g_i^c(\mathbf{x},t) = g_i^{c,eq}(\mathbf{x},t) + g_i^{c,neq}(\mathbf{x}_a,t) \tag{27}$$

where $f_i^{c,eq}$ and $g_i^{c,eq}$ are the equilibrium distributions calculated from Eqs. (6) and (7), $f_i^{c,neq}$ and $g_i^{c,neq}$ are the non-equilibrium distributions on coarse grid x_a and can be obtained from:

$$f_i^{c,neq}(\mathbf{x}_a,t) = f_i(\mathbf{x}_a,t) - f_i^{eq}(\mathbf{x}_a,t) \tag{28}$$

$$g_i^{c,neq}(\mathbf{x}_a,t) = g_i(\mathbf{x}_a,t) - g_i^{eq}(\mathbf{x}_a,t) \tag{29}$$

where $\mathbf{x}_a$ is site of the adjacent inner coarse grid. It is noted that the non-equilibrium extrapolation scheme has the second-order accuracy and good numerical stability. In the paper we will use such treatment to the artificial boundary.

2.3.2. Coupling transition from the coarse mesh region to the fine mesh region

As mentioned above, a time step Δt^c for the coarse region corresponds to n time steps Δt^f for the fine region and a coarse spatial step $\Delta \mathbf{x}^c$ contains n fine spatial steps $\Delta \mathbf{x}^f$. Thus, the interim or temporary information at a series of fine time and special steps is lacking for the coupling from the coarse region to the fine region and the interpolation processes are needed. For the sake of simplicity, the linear interpolation algorithm is used on the temporal steps and the second-order parabolic interpolation is adopted for the spatial interpolation process. Since the calculation steps start up from the coarse mesh region, so one first gets the relevant variables and parameters on the coarse grids at the time of $t + \Delta t^c$. At the same time, the physical variables on the fine mesh boundary which also lies in the inner of the coarse meshes can be obtained the values at time $t + \Delta t^c$. Then, by means of the temporal interpolation between the time of t and $t + \Delta t^c$ as well as the spatial interpolation, one will get the physical parameters of mixed fluid on the fine mesh boundary at the relevant time. And then by some assumptions, the physical parameters (velocity, density and temperature) of each component could be obtained. Finally, by means of non-equilibrium extrapolation scheme, the post-collision distribution functions of each component of the nanofluid on the fine mesh boundary can be achieved. The concrete description of interpolation processes are as follows.

The temporal interpolation from the physical parameters of the mixed fluid between t and $t + \Delta t^c$ on the coarse grids provides the relevant information corresponding to k time steps $k\Delta t^f$ ($k = 1, 2, \ldots, n$) on the fine mesh boundary:

$$\rho^f(\mathbf{x}, t + k\Delta t^f) = \left(1 - \frac{k}{n}\right)\rho^c(\mathbf{x}, t) + \frac{k}{n}\rho^c(\mathbf{x}, t + \Delta t^c) \tag{30}$$

$$u^f(\mathbf{x}, t + k\Delta t^f) = \left(1 - \frac{k}{n}\right)u^c(\mathbf{x}, t) + \frac{k}{n}u^c(\mathbf{x}, t + \Delta t^c) \tag{31}$$

$$T^f(\mathbf{x}, t + k\Delta t^f) = \left(1 - \frac{k}{n}\right)T^c(\mathbf{x}, t) + \frac{k}{n}T^c(\mathbf{x}, t + \Delta t^c) \tag{32}$$

By the spatial interpolation on coarse grids, we obtain the relevant values of mix fluid at $x + l\Delta x^f$ ($l = 1, 2, \ldots, n$) on the fine mesh boundary:

$$\begin{aligned}\rho^f(\mathbf{x} + l\Delta \mathbf{x}^f, t + k\Delta t^f) = {} & a(1) \times \rho^c(\mathbf{x} - \Delta x^c, t + k\Delta t^f) + a(2) \\ & \times \rho^c(\mathbf{x}, t + k\Delta t^f) + a(3) \\ & \times \rho^c(\mathbf{x} + \Delta \mathbf{x}^c, t + k\Delta t^f)\end{aligned} \tag{33}$$

$$\begin{aligned}\mathbf{u}^f(\mathbf{x} + l\Delta \mathbf{x}^f, t + k\Delta t^f) = {} & a(1) \times \mathbf{u}^c(\mathbf{x} - \Delta \mathbf{x}^c, t + k\Delta t^f) + a(2) \\ & \times \mathbf{u}^c(\mathbf{x}, t + k\Delta t^f) + a(3) \\ & \times \mathbf{u}^c(\mathbf{x} + \Delta \mathbf{x}^c, t + k\Delta t^f)\end{aligned} \tag{34}$$

$$\begin{aligned}T^f(\mathbf{x} + l\Delta \mathbf{x}^f, t + k\Delta t^f) = {} & a(1) \times T^c(\mathbf{x} - \Delta \mathbf{x}^c, t + k\Delta t^f) + a(2) \\ & \times T^c(\mathbf{x}, t + k\Delta t^f) + a(3) \\ & \times T^c(\mathbf{x} + \Delta x^c, t + k\Delta t^f)\end{aligned} \tag{35}$$

where $a(1) = -\frac{l\Delta \mathbf{x}^f(\Delta \mathbf{x}_c - l\Delta \mathbf{x}^f)}{2\Delta \mathbf{x}_c^2}$, $a(2) = \frac{(\Delta \mathbf{x}_c - l\Delta \mathbf{x}^f)(\Delta \mathbf{x}_c + l\Delta \mathbf{x}^f)}{\Delta \mathbf{x}_c^2}$, and $a(3) = \frac{l\Delta \mathbf{x}^f(\Delta \mathbf{x}_c + l\Delta \mathbf{x}^f)}{2\Delta \mathbf{x}_c^2}$.

Then, considering the slip velocity of each component α, the equilibrium velocity of component α on the fine mesh boundary is modified as:

$$\mathbf{u}^{f,\alpha}(\mathbf{x} + l\Delta \mathbf{x}^f, t + k\Delta t^f) = \mathbf{u}^f(\mathbf{x} + l\Delta \mathbf{x}^f, t + k\Delta t^f) + \Delta \mathbf{u}^\alpha(\mathbf{x}_a, t + k\Delta t^f) \tag{36}$$

where x_a is site of the adjacent inner fine grid and Δu^α is the slip velocity given in Eq. (21).

Here it should be emphasized that as indicated by the relationship in Eq. (2), the speed of sound is assumed to be constant on different meshes. This expression elucidates the same wrapped relationship for both the spatial steps and the temporal steps corresponding to different scale regions, which means that the number of the spatial interpolation steps is equal to that of the temporal interpolation steps. Therefore, the same refinement parameter n is introduced for both the spatial and temporal interpolation. Once the density distribution of the mixed fluid ρ^f is known, the density distributions of nanoparticle phase ρ^P and the base fluid phase ρ^L can be calculated from:

$$\rho^P(\mathbf{x} + l\Delta \mathbf{x}^f, t + k\Delta t^f) = (\rho^f(\mathbf{x} + l\Delta \mathbf{x}^f, t + k\Delta t^f) - \rho_L)/(\rho_p - \rho_L) \times \rho_p \tag{37}$$

$$\begin{aligned}\rho^L(\mathbf{x} + l\Delta \mathbf{x}^f, t + k\Delta t^f) = {} & (1.0 - (\rho^f(\mathbf{x} + l\Delta \mathbf{x}^f, t + k\Delta t^f) \\ & - \rho_L)/(\rho_p - \rho_L)) \times \rho_L\end{aligned} \tag{38}$$

where ρ_p and ρ_L are the density of pure nanoparticles and base fluid, respectively.

Based on the assumption that the temperatures of all components are equal to the mixture temperature in the hybrid region, one has:

$$T^\alpha(\mathbf{x} + l\Delta \mathbf{x}^f, t + k\Delta t^f) = T^f(\mathbf{x} + l\Delta \mathbf{x}^f, t + k\Delta t^f) \tag{39}$$

Thus, the post-collision distribution functions of each component of the nanofluid on the fine mesh boundary can be calculated by the non-equilibrium extrapolation scheme (Guo et al., 2002b):

$$f_i^{f,\alpha}(x, t) = f_i^{f,eq,\alpha}(u^{f,\alpha}(x, t), \rho^\alpha(x, t)) + f_i^{f,neq,\alpha}(u^{f,\alpha}(x_a, t), \rho^\alpha(x_a, t)) \tag{40}$$

$$g_i^{f,\alpha}(x, t) = g_i^{f,eq,\alpha}(u^{f,\alpha}(x, t), \rho^\alpha(x, t), T^\alpha(x, t)) + g_i^{f,neq,\alpha}(u^{f,\alpha}(x_a, t), \rho^\alpha(x_a, t)) \tag{41}$$

here $f_i^{f,eq,\alpha}$ and $g_i^{f,eq,\alpha}$ are the equilibrium distributions calculated by Eqs. (14) and (15). $f_i^{f,neq,\alpha}$ and $g_i^{f,neq,\alpha}$ are the non-equilibrium distributions on the adjacent fine grid x_a. $f_i^{f,neq,\alpha}(x_a, t) = f_i^{f,\alpha}(x_a, t) - f_i^{f,eq,\alpha}(x_a, t)$ and $g_i^{f,neq,\alpha}(x_a, t) = g_i^{f,\alpha}(x_a, t) - g_i^{f,eq,\alpha}(x_a, t)$.

2.4. Computational steps

The basic algorithm steps of the hybrid simulation:

(1) streaming $f_i(\mathbf{x}, t)$ and $g_i(\mathbf{x}, t)$ on inner coarse grids;

(2) calculating the physical parameters $\rho(\mathbf{x} + \Delta \mathbf{x}^c, t + \Delta t^c)$, $u(\mathbf{x} + \Delta \mathbf{x}^c, t + \Delta t^c)$, and $T(\mathbf{x} + \Delta \mathbf{x}^c, t + \Delta t^c)$ on inner coarse grids and then getting the post-collision distribution functions $f_i^\alpha(\mathbf{x} + \Delta \mathbf{x}^c, t + \Delta t^c)$ and $g_i^\alpha(\mathbf{x} + \Delta \mathbf{x}^c, t + \Delta t^c)$;

(3) conducting the spatial and temporal interpolation to get the values of $\rho^{f,\alpha}(\mathbf{x} + l\Delta \mathbf{x}^f, t + k\Delta t^f)$, $u^{f,\alpha}(\mathbf{x} + l\Delta \mathbf{x}^f, t + k\Delta t^f)$, and $T^{f,\alpha}(\mathbf{x} + l\Delta \mathbf{x}^f, t + k\Delta t^f)$, and then obtaining the post-collision distribution functions $f_i^\alpha(\mathbf{x} + l\Delta \mathbf{x}^f, t + k\Delta t^f)$ and $g_i^\alpha(\mathbf{x} + l\Delta \mathbf{x}^f, t + k\Delta t^f)$ on the fine mesh boundary by Eqs. (40) and (41);

(4) carrying out computation for n times to find f_i^α, g_i^α, $\rho^\alpha(\mathbf{x} + \Delta \mathbf{x}^f, t + \Delta t^c)$, $\mathbf{u}^\alpha(\mathbf{x} + \Delta \mathbf{x}^f, t + \Delta t^c)$, and $T^\alpha(\mathbf{x} + \Delta \mathbf{x}^f, t + \Delta t^c)$ on inner fine grids;

(5) integrating $\rho^\alpha(\mathbf{x} + \Delta \mathbf{x}^f, t + \Delta t^c)$, $u^\alpha(\mathbf{x} + \Delta \mathbf{x}^f, t + \Delta t^c)$, and $T^\alpha(\mathbf{x} + \Delta \mathbf{x}^f, t + \Delta t^c)$ along the coarse mesh boundary to obtain $\rho(\mathbf{x} + \Delta \mathbf{x}^c, t + \Delta t^c)$, $\mathbf{u}(\mathbf{x} + \Delta \mathbf{x}^c, t + \Delta t^c)$, $T(\mathbf{x} + \Delta \mathbf{x}^c, t + \Delta t^c)$, and then

by Eqs. (28) and (29) get the post-collision distribution functions $f_i^z(x+\Delta x^c, t+\Delta t^c)$ and $g_i^z(x+\Delta x^c, t+\Delta t^c)$ on coarse mesh boundary; and

(6) returning to step 1 for a new circulation.

2.5. Forces and potentials in a nanofluid

Keep in mind that the two-component feature of the nanofluid in the fine mesh region is vital and one can handle the interaction between the nanoparticles component and the ambient base liquid as well as the interparticles action by means of a series of forces and potentials. Since the nanofluid can be considered as a type of the colloidal suspension, one can use the colloid theory to describe the dynamics of the suspended nanoparticles. Several internal and external forces or potentials are exerted on the nanofluid system such as the buoyancy and the gravitational force $\mathbf{F}_H$, the interaction potential $\mathbf{F}_A$ among the nanoparticles, the drag force $\mathbf{F}_D$, and the Brownian force F_i. By summing up all these forces on each particle and multiplying the number of particles on each grid, the total forces on each grid will be obtained. Here we give the brief introduction to these forces and the detailed expressions have been discussed in the previous work (Xuan and Yao, 2005).

The buoyancy and gravity force is given as:

$$\mathbf{F}_H = -\frac{1}{6}\pi d_p^3 g \Delta\rho' \tag{42}$$

where d_p is the diameter of the nanoparticle and $\Delta\rho'$ is the mass density difference between the suspended nanoparticle and the base fluid.

The drag force (Stokes force) is:

$$\mathbf{F}_D = -3\pi d_p \mu \Delta\mathbf{u} \tag{43}$$

where μ is the viscosity of the fluid and $\Delta\mathbf{u}$ is the velocity difference between the particle and the base fluid.

The interactions potential between the nearest neighbor nanoparticles is (Russel et al., 1989):

$$V_A = -\frac{1}{6}A\left(\frac{2a^2}{L^2-4a^2}+\frac{2a^2}{L^2}+\ln\frac{L^2-4a^2}{L^2}\right) \tag{44}$$

where L is the center-to-center distance between particles, and A is the Hamaker constant which accounts for the material properties independent of the geometrical shape. For all of the nanoparticles within the adjacent lattices in the D2Q9 model, the force caused by the interaction potential is written as:

$$\mathbf{F}_A = \sum_{i=1}^{8} N_i \frac{\partial V_A}{\partial \mathbf{r}_i} \tag{45}$$

where N is the number of the particles within the adjacent lattice i, $N = \rho^p V^f / m_p$ (m_p is the mass of a single nanoparticle).

Although the Brownian motion is irregular, the Brown force can be considered as the comprehensive effect of the actions exerted by the surrounding molecules of the fluid and the thermal energy. Since Brownian motion is generally simulated as a Gaussian white-noise process, the algorithm for simulating the Brownian force is similar to that for generating a white-noise process modeled as a Gaussian white-noise process (He and Ahmadi, 1999):

$$\mathbf{F}_i(t) = G_i\sqrt{C/dt} \tag{46}$$

where the parameter G_i is a Gaussian random number with zero mean and unit variance, and $C = 6\pi\mu d_p k_B T$.

Thus, the vector sum of the total forces acting on the nanoparticles component per unit lattice volume is:

$$\mathbf{F}^p = N(\mathbf{F}_A + \mathbf{F}_i + \mathbf{F}_D + \mathbf{F}_H)/V \tag{47}$$

where N is the number of the particles in a given lattice and V is the lattice volume. On the other hand, the forces act on the fluid molecules in a given lattice can be expressed as reaction of the drag force and Brownian force:

$$\mathbf{F}^w = -N(\mathbf{F}_i + \mathbf{F}_D) \tag{48}$$

It is emphasized that the sum of some forces is equal to zero for the single mixed fluid in the coarse region because of the fact that they are intra forces within the system and appear in pair with opposite signs. For the coarse region, only the forces induced by the external fields such as the buoyancy and the gravitational force $\mathbf{F}_H$ need to be treated in the model. On the other hand, all the internal and external forces as well as potentials must separately handled for each component in the fine region.

3. Results and discussion

In this section, two simple examples are introduced to show how to apply the above-described multiscale simulation approach to the flow and energy transport processes of nanofluids inside a microchannel. The first one is a sudden-start Couette flow. For the case of larger shear force may appear nearby the moving upper plate at the startup process, the MLBM with fine meshes will be applied in the region near the upper plate. The other example is the convection in a parallel plate channels with the high constant temperature on the top plate, and the fine meshes nearby the top plate are used for exactly simulating the heat transfer process. From these two examples, the accuracy of the hybrid method will be discussed and the flow and energy transfer characteristic of nanofluid will be investigated at the same time.

3.1. Sudden-start Couette flow

A sudden-start Couette flow of the Cu-water nanofluid with the volume fraction of 1% Cu nanoparticles whose diameter is 10 nm in the microchannel is simulated. The density of Cu nanoparticles and the base fluid is $\rho_p = 8930\ \mathrm{kg/m^3}$ and $\rho_L = 997\ \mathrm{kg/m^3}$, respectively. The viscosity of the nanofluid is $\nu = 1.2\times10^{-6}\ \mathrm{m^2/s}$. The fluid is confined between two parallel plates with the distance of $L_y = 50\ \mu\mathrm{m}$, and the fluid temperature is 300 K. Initially, the fluid velocity is assumed to be zero. At $t = 0$, the upper plate begins to move at a constant velocity $u_0 = 0.01$ m/s, while the bottom plate is fixed. As shown in Fig. 4, the MLBM with fine meshes is applied in the region nearby the moving upper plate ($y > 42\ \mu\mathrm{m}$), the SLBM

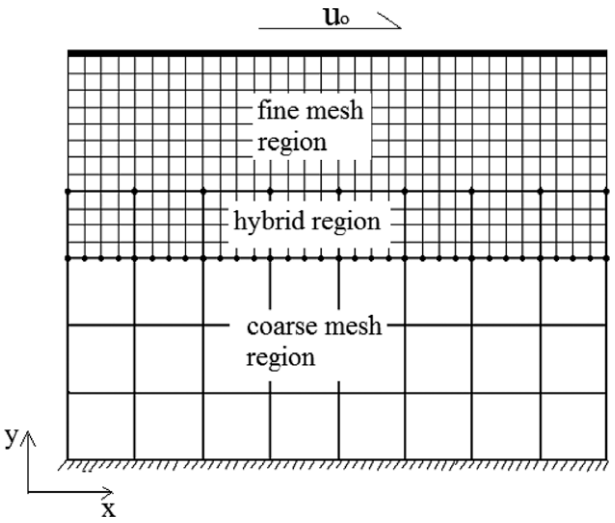

Fig. 4. Schematic of Couette flow.

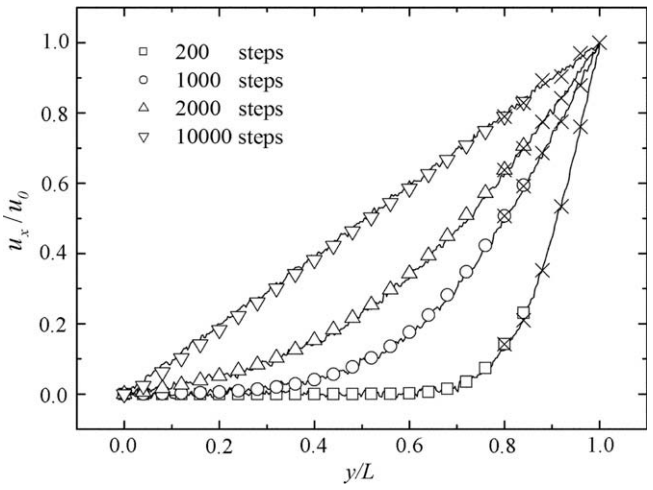

Fig. 5. Horizontal velocity u_x as a function of y (the hybrid results of the single-component method portion and multi-component method portion are respectively shown with hollows and asterisks and the results from the pure MLBM are shown with line).

with coarse meshes is applied to most region of the channel ($y < 40$ μm) and the overlap region will be simulated by both the SLBM and MLBM ($40\ \mu m \leqslant y \leqslant 42\ \mu m$). Periodic boundary conditions are used at the entrance and exit of the channel in the x direction. In addition, no-slip boundary conditions are imposed at both the top and the bottom. The spatial steps and the time steps are: $\Delta x^c = 2 \times 10^{-6}$ m, $\Delta t^c = 1 \times 10^{-7}$ s, $\Delta x^f = \Delta x^c/16$, and $\Delta t^f = \Delta t^c/16$, and the refinement parameter is $n = 16$. The relaxation-time factors τ^c and τ^f are given as 0.59 and 1.94 for the coarse mesh region and the fine mesh region, respectively.

3.1.1. The continuity of physical information on the hybrid region

Fig. 5 shows the velocity profiles at different time of sudden-start Couette flow obtained by both the hybrid method and the pure MLBM. The hybrid results of the single-component method portion and multi-component method portion are shown by hollows and asterisks, respectively, and the pure MLBM result is shown by the line. The velocity of mixed fluid on the fine mesh region is calculated by Eq. (20). At the beginning, only the upper region of the fluid experiences the drag effect from the upper plate. Later, the steady state linear Couette profile is formed. It is shown that the results of hybrid method and the pure MLBM agree well. Furthermore, the result of single-component method portion and multi-component method portion of the MSHM track closely in the overlap region. This demonstrates that the continuity of physical parameters at the hybrid interface can be assured by using the present hybrid method.

3.1.2. The fluid features and morphology of nanofluid on different scales

The flow features of nanofluid on different mesh scales at $t = 2 \times 10^{-4}$ s are shown in Fig. 6. On coarse mesh scale the velocity

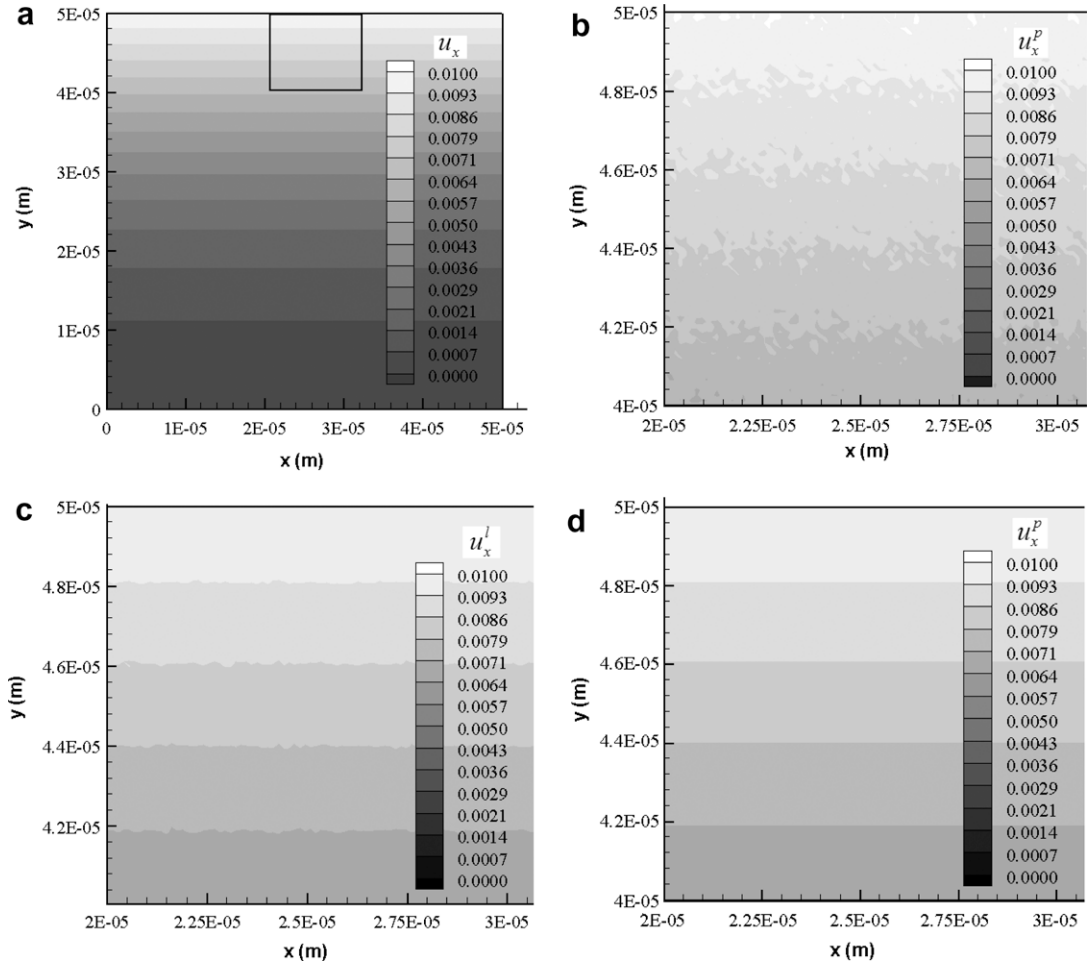

Fig. 6. Distributions of velocities (a) u_x of the mixed nanofluid on coarse mesh scale (b) u_x^p of nanoparticle component on fine mesh scale (c) u_x^f of base liquid component on fine mesh scale and (d) u_x^p of nanoparticle component on fine mesh scale without considering the internal and external forces.

u_x of mixed fluid is invariable along the x direction as shown in Fig. 6a. On the fine mesh scale, u_x^p of the nanoparticle component shows obvious fluctuation along the x direction (as shown in Fig. 6b). Compared with the u_x^l distribution of base liquid (as shown in Fig. 6c), u_x^p of nanoparticle component presents more asymmetric characteristic. For analyzing the velocity fluctuation on the fine mesh scale, we simulate the same case with the hybrid method by neglecting the forces given in Eqs. (42)–(46). The results indicate that such fluctuation disappears (as shown in Fig. 6d). Thus, we can affirm that the fluctuation mainly results from the complicated forces acting on the suspended nanoparticles.

Fig. 7 shows the morphologic characteristics of nanofluid on different scales, in which the vertical coordinate on the right-hand side denotes the density of the nanofluid. For the case that the volume fraction of Cu nanoparticles is 1%, the average density of the Cu-water nanofluid is 1076.33 kg/m^3. As shown in Fig. 7a, on the coarse mesh scale the density distribution of the mixed fluid ρ fluctuates within the span of 0.0001 kg/m^3, while on the fine mesh scale the fluctuant span of nanoparticles density ρ^p is 0.0067 kg/m^3 (as shown in Fig. 7b). The density fluctuation of the nanofluid may due to that the present hybrid method has considered the complicated forces acting on each component of nanofluid. This fluctuation was also indicated in the previous work (Xuan and Yao, 2005). The refinement parameter n also influences the density distribution feature. The simulation results for $n = 5$ are shown in Fig. 7c and d. Comparing Fig. 7a and b with Fig. 7c and d, one will find that on the coarse mesh scale the density fluctuations of mixed fluid are similar for different refinement n, but at the fine mesh scale the density fluctuations of nanoparticle component increase with the refinement n. The reason is due to the fact that with the increase of refinement n, the multiphase characteristic of nanofluid becomes more and more protrudent. It is emphasized that all the fluctuations of densities and velocities may influence the heat transfer process, and we will discuss the convection of nanofluid in the next section.

3.2. Convection within parallel plate channels

To investigate the heat transfer features of nanofluid, a laminar flow in a channel within parallel plates is simulated. The fluid used in the simulation is the Cu–Water nanofluid with the volume fraction of 1% Cu nanoparticles whose diameter is 10 nm. The length of the simulation domain is $L_x = 40$ μm and the width $L_y = 20$ μm. An external force $F_x = 2 \times 10^6$ N/m^3 along the x direction is introduced as a driving force. Initially, the nanofluid is stationary and the fluid temperature is assumed to $T_0 = 300$ K. The dimensionless temperature is defined as: $T^* = (T - T_0)/(T_{up} - T_0)$, where T_{up} is the constant temperature of top plate, $T_{up} = 350$ K. Obviously, the dimensionless temperature of the top plate is $T_w^* = 1$ and the inlet temperature of the nanofluid is $T_{in}^* = 0$, the bottom plate is insulated. In the region of $y < 10$ μm, the SLBM is applied with $\Delta \mathbf{x}^c = 1 \times 10^{-6}$ m, $\Delta t^c = 5 \times 10^{-8}$ s. In the region of $y > 11$ μm, the MLBM is used with $\Delta \mathbf{x}^f = 0.125 \times 10^{-6}$ m, $\Delta t^f = 0.625 \times 10^{-8}$ s, The relaxation-time factors τ^c and τ^f are set to be 0.68 and 1.94, and the thermal relaxation-time factor are $\tau_T^c = 0.5162$ and $\tau_T^f = 0.6297$, respectively. The overlapped region ($10\ \mu m \leqslant y \leqslant 11\ \mu m$) is described by the both SLBM and MLBM.

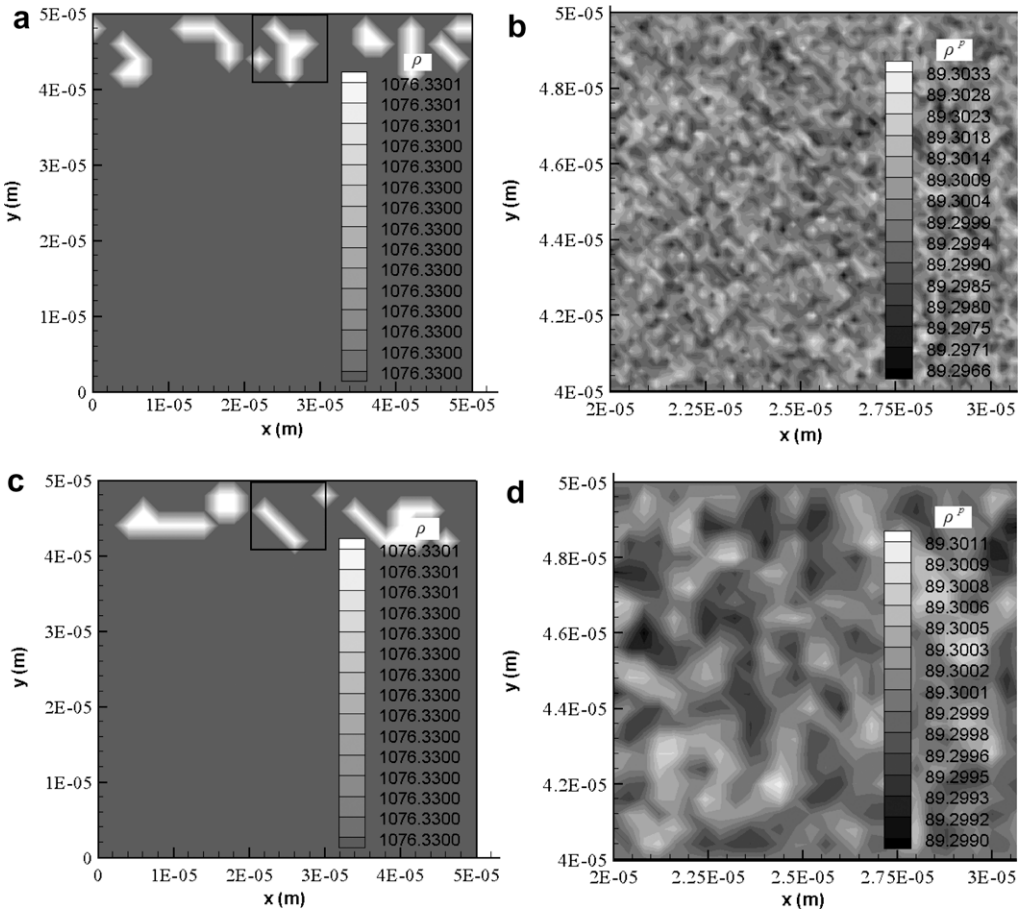

Fig. 7. Density distribution (a) density of mixed nanofluid on coarse mesh scale, $n = 16$ (b) density of nanoparticles on fine mesh scale, $n = 16$ (c) density of mixed nanofluid on coarse mesh scale, $n = 5$ and (d) density of nanoparticles on fine mesh scale, $n = 5$.

3.2.1. Temperature distribution of nanofluid

Fig. 8 shows the temperature distribution obtained from different approaches at $t = 1 \times 10^{-4}$ s. Fig. 8a and c correspond to the temperature distribution of the nanofluid by the MSHM and pure MLBM approaches, respectively. Fig. 8b shows the temperature distribution of the nanofluid obtained from the pure SLBM approach. The size of coarse grids used in the MSHM is the same as that for the SLBM and the size of fine grids used in the hybrid method is equal to that in the MLBM. By comparing Fig. 8a or c with Fig. 8b, one can find that in the inlet region the isotherm is acute. This may be that the MSHM or pure MLBM considers the internal forces between nanoparticles and base fluid and these forces induce fluctuation of the velocities and densities nanofluid, so that the heat transfer process is locally enhanced. To quantitatively investigate the heat transfer process of nanofluid, the Nussle number *Nu* is introduced and discussed in the following.

3.2.2. The Nusselt number with different approaches

The Nusselt number *Nu* is defined as:

$$Nu(x) = \frac{h(x)L_y}{k} = \frac{L_y}{[T_w(x) - T_b(x)]}\left(\frac{\partial T}{\partial y}\right)_{y=L_y} \tag{49}$$

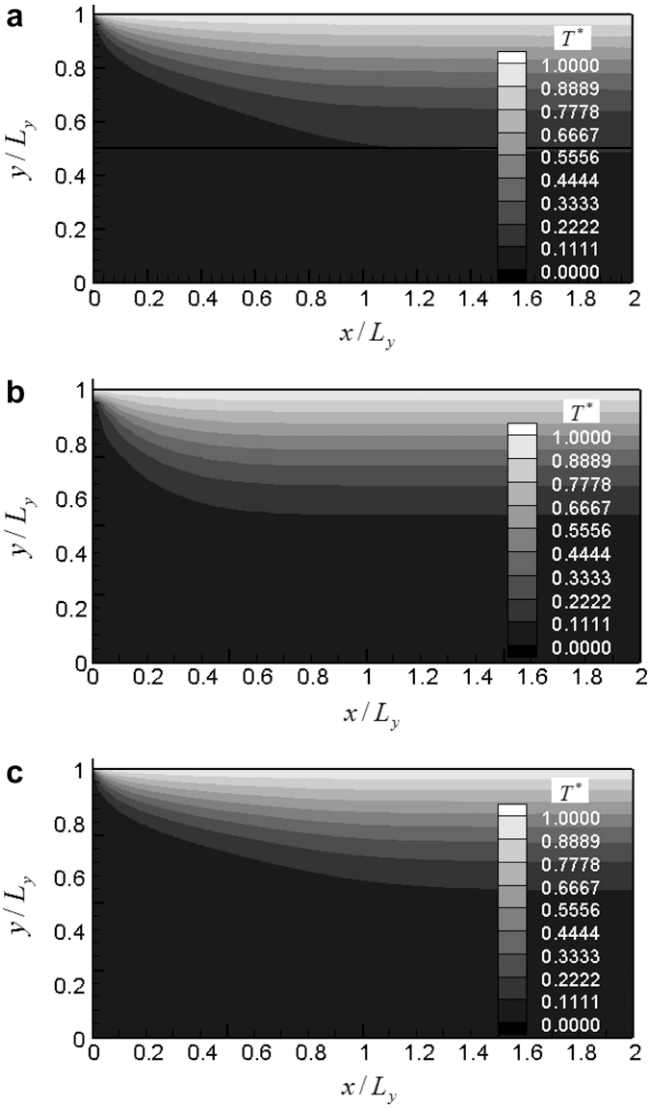

Fig. 8. Temperature distribution (a) temperature of nanofluid obtained from the MSHM approach (b) temperature of nanofluid from the Pure SLBM and (c) Temperature of nanofluid from the MLBM.

where $h(x)$ is the local convective heat transfer coefficient, k is the thermal conductivity of nanofluid, and $T_b(x)$ is the average temperature of mixed fluid at position x.

Fig. 9 respectively presents the Nusselt number *Nu* values obtained by using MSHM, pure SLBM and pure MLBM as well as the Nusselt number of pure water by SLBM at $t = 1 \times 10^{-4}$ s. As shown in Fig. 9, the values of the Nusselt number obtained by using different approaches show almost the same tendency near the entrance and diminish rapidly along the flow direction and finally reach a constant. Compared with pure water, the averaged *Nu* of nanofluid obtained from the MSHM increases about 8.34%. The remarkable enhancement appears at the entrance region ($0 < x/L_x < 0.3$) and reaches about 12.16% and then such tendency is retarded along with the axial distance. Numerical simulation from the SLBM approach shows that the *Nu* of nanofluid also increases compared with that of pure water. The enhancement tendency agrees well with the experimental data (Wen and Ding, 2004). From Fig. 9, one can also find that the *Nu* obtained from the MSHM approach coincides well with that from the MLBM. But the latter one will cost much more computation time. It reminds us of the fact that although the MLBM can accurately simulate the flow and energy transfer process but it will cost much more computation time compared with the MSHM approach. In the next section we will discuss the computational efficiency of MSHM.

4. Computational efficiency analysis

A high computational efficiency is very significant for a numerical approach, so that it is necessary to investigate the factors which may affect the computational efficiency. The efficiency of the hybrid method is mainly dominated by the refinement parameter n and Φ (Φ is the ratio of the volume treated with multi-component method to the total volume of the whole region). In this section we discuss the relationship between computation efficiency from the numerical results of the sudden-start Couette flow corresponding to the Pentium(R) 4 CPU 3.00 GHz processor. The computational convergence criterion is given as:

$$\frac{\sum_{i,j}|u_x(t) - u_x(t - \Delta t)|}{\sum_{i,j}|u_x(t)|} < 10^{-6} \tag{50}$$

Fig. 10 shows the computational time related with refinement parameter n for different approaches. The coarse grid size used in the hybrid method is the same as that in the pure SLBM and the fine grid size used in the hybrid method is equal to that in the pure

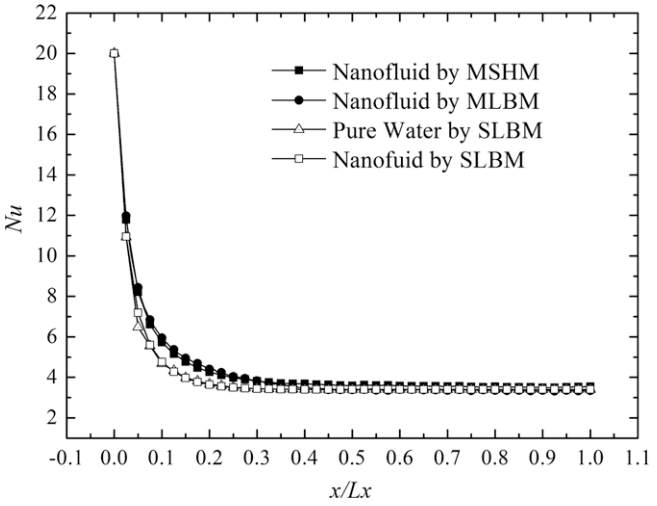

Fig. 9. *Nu* along the *x* direction.

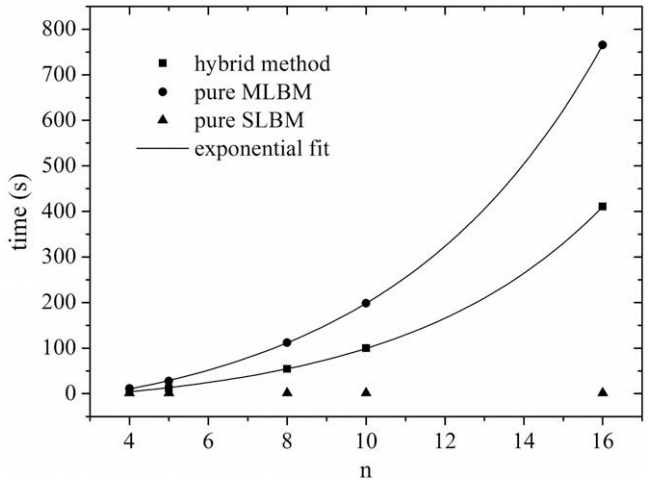

Fig. 10. The relation between computation time and refinement parameter n.

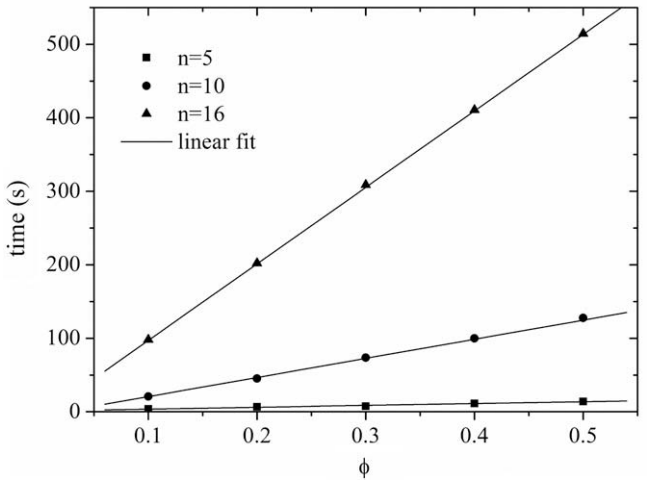

Fig. 11. The relation between computation time and Φ.

MLBM approach. Here Φ is set to be 40%. The results indicate that the pure MLBM consumes the maximum computational time and the hybrid method used less time compared with the pure MLBM. The computational time for either the hybrid approach or the pure MLBM exponentially increases with the refinement parameter n as shown in Fig. 10. Thus, the hybrid approach can remarkably reduce the computational time compared with the MLBM, and it is more important for bigger refinement parameter n.

Fig. 11 shows the computational time consumed by the hybrid method for different values of parameter Φ. One can find that the computational time increases linearly with Φ. As the computation region corresponding to the MLBM approach increases by five times (i.e., parameter Φ increases from 0.1 to 0.5), the consumed computation time increases more than 5-fold for the case of $n = 16$. It indicates that the total computational time is mainly determined by the region ratio where the MLBM is applied. There exists compromise between the MLBM application portion of the solution region and the affordable computational time.

5. Conclusions

Based on the lattice Boltzmann method, a novel multicomponent and single-component hybrid method (MSHM) for the nanofluid has been proposed, in which the multicomponent lattice Boltzmann model is used in interfacial regions where the velocity or temperature change rapidly and the single-component lattice Boltzmann model is applied in the region where the nanofluid can be treated as a single mixed fluid. The simulation results for the Couette flow and convection within a channel confined between two parallel plates have shown that on the coarse grid scale the conservation principles of mass, momentum and energy along the hybrid boundary of the MSHM approach can be guaranteed and the accuracy of numerical results from the MSHM can be assured.

As the refinement parameter n increases, the computational results will more clearly reveal the multiphase feature of nanofluid in the fine mesh region. The computational time of the MSHM increases linearly with the parameter Φ and exponentially with the refinement parameter n. The presented hybrid approach is more efficient than the pure MLBM with the acceptable accuracy, which may be of great significance for improving our understanding of the flow and heat transfer process of nanofluids.

Acknowledgment

This work is sponsored by the National Natural Science Foundation of China (Grant No. 50436020).

References

Ahrenholz, B., Toelke, J., Krafczyk, M., 2006. Lattice-Boltzmann simulations in reconstructed parametrized porous media. Int. J. Comput. Fluid D 20, 369–377.
Arulmurugan, R., Vaidyanathan, G., Sendhilnathan, S., Jeyadevan, B., 2005. Preparation and properties of temperature-sensitive magnetic fluid having Co0.5Zn0.5Fe2O4 and Mn0.5Zn0.5Fe2O4 nanoparticles. Physica B 368, 223–230.
Cao, N., Chen, S., Jin, S., Martinez, D., 1997. Physical symmetry and lattice symmetry in the lattice Boltzmann method. Phys. Rev. E 55, 22–24.
Chen, H., Filippova, O., Hoch, J., Molvig, K., Shock, R., Teixeira, C., Zhang, R., 2006. Grid refinement in lattice Boltzmann methods based on volumetric formulation. Physica A 362, 158–167.
Choi, U.S., 1995. Enhancing thermal conductivity of fluids with nanoparticles. ASME FED 231, 99–103.
Das, S., Putra, N., Roetzel, W., 2003. Pool boiling of nano-fluids on horizontal narrow tubes. Int. J. Multiphase Flow 29, 1237–1247.
Das, S., Choi, S., Patel, H., 2006. Heat transfer in nanofluids—a review. Heat Transfer Eng. 27, 3–19.
Dellar, P., 2002. Lattice Kinetic Schemes for Magnetohydrodynamics. J. Comput. Phys. 179, 95–126.
Dupuis, A., Chopard, B., 2003. Theory and applications of an alternative lattice Boltzmann grid refinement algorithm. Phys. Rev. E 67, 066707.
Enomoto, Y., Oba, K., Okada, M., 2003. Simulation study on microstructure formations in magnetic fluids. Physica A 330, 496–506.
Filippova, O., Haenel, D., 1998. Grid refinement for lattice-BGK models. J. Comput. Phys. 147, 219–228.
Guo, Z., Shi, B., Zheng, C., 2002a. A coupled lattice BGK model for the Bouessinesq equation. Int. J. Numer. Methods Fluid 39, 325–342.
Guo, Z., Zheng, C., Shi, B., 2002b. Non-equilibrium extrapolation method for velocity and pressure boundary conditions in the lattice Boltzmann method. Chinese Phys. 11, 366–374.
He, C., Ahmadi, G., 1999. Particle deposition in a nearly developed turbulent duct flow with electrophoresis. J. Aerosol Sci. 30, 739–758.
He, X., Luo, L., Dembo, M., 1996. Some progress in lattice Boltzmann method part 1. Nonuniform mesh Grids. J. Comput. Phys. 129, 357–362.
Higuera, F.J., Succi, S., Benzi, R., 1989. Lattice gas dynamics with enhanced collisions. Europhys. Lett. 9, 345–349.
Higuere, F., Jimenez, J., 1989. Boltzmann approach to lattice gas simulations. Europhys. Lett. 9, 663–668.
Hortmann, M., Peric, M., Scheuerer, G., 1990. Finite volume multigrid prediction of laminar natural convection: bench-mark solutions. Int. J. Numer. Methods Fluids 11, 189–207.
Kandhai, D., Soll, W., Chen, S., Hoekstra, A., Sloot, P., 2000. Finite-difference lattice-BGK methods on nested grids. Comput. Phys. Commun. 129, 100–109.
Kim, P., Shi, L., Majumdar, A., McEuen, P.L., 2001. Thermal transport measurements of individual multiwalled nanotubes. Phys. Rev. Lett. 87, 215502-1-4.
Kwon, Y., Hosoglu, S., 2008. Application of lattice Boltzmann method, finite element method, and cellular automata and their coupling to wave propagation problems. Comput. Struct. 86, 663–670.
Lee, S., Choi, S.U.S., Li, S., Eastman, J.A., 1999. Measuring thermal conductivity of fluids containing oxide nanoparticles, transactions of ASME. J. Heat Trans. 121, 280–289.
Li, Y., Eugene, J., LeBoeuf, Basu, P., 2004. Least-squares finite-element lattice Boltzmann method. Phys. Rev. E 69, 065701(R).

Li, Q., He, Y., Wang, Y., Tao, W., 2007. Coupled double-distribution-function lattice Boltzmann method for the compressible Navier–Stokes equations. Phys. Rev. E 76, 056705.
Love, P., Nekovee, M., Coveney, P., Chin, J., González-Segredo, N., Martin, J., 2003. Simulations of amphiphilic fluids using mesoscale lattice-Boltzmann and lattice-gas methods. Comput. Phys. Commun. 153, 340–358.
Massaioli, F., 1993. Exponential tails in two-dimensional Rayleigh-Bénard Convection. Europhys. Lett. 21, 305–310.
McNamara, G.R., Zanetti, G., 1988. Use of the Boltzmann equation to simulate lattice-gas automata. Phys. Rev. Lett. 61, 2332–2335.
Nannelli, F., Succi, S., 1992. The lattice Boltzmann equation on irregular lattices. J. Stat. Phys. 68, 401–407.
Nie, X.B., Chen, S.Y., E, W.N., Robbins, M.O., 2004. A continuum and molecular dynamics hybrid method for micro- and nano-fluid flow. J. Fluid Mech. 500, 55–64.
Pan, C., Hilpert, M., Miller, C., 2004. Lattice-Boltzmann simulation of two-phase flow in porous media. Water Resour. Res. 40, 1–14.
Patil, Dhiraj V., Lakshmisha, K.N., 2009. Finite volume TVD formulation of lattice Boltzmann simulation on unstructured mesh. J. Comput. Phys. 228, 5262–5279.
Russel, W.B., Saville, D.A., Schowalter, W.R., 1989. Colloidal Dispersion. Cambridge University Press, Cambridge.
Shan, X., 1997. Simulation of Rayleigh-Benard convection using a lattice Boltzmann method. Phys. Rev. E 55, 2780–2788.
Shan, X., Chen, H., 1993. Lattice Boltzmann model for simulating flows with multiple phases and components. Phys. Rev. E 47, 1815–1819.
Shan, X., Doolen, G., 1995. Multicomponent lattice-Boltzmann with interparticle interaction. J. Stat. Phys. 81, 379–393.
Shu, C., Chew, Y.T., Niu, X.D., 2001. Least square-based LBM: a meshless approach for simulation of flows with complex geometry. Phys. Rev. E 64, 1–4.
Sofonea, V., Frueh, W., 2001. Lattice Boltzmann model for magnetic fluid interfaces. Eur. Phys. J. B 20, 141–149.
Stiebler, M., Tölke, J., Krafczyk, M., 2006. An upwind discretization scheme for the finite volume lattice Boltzmann method. Comput. Fluids 35, 814–819.
Swift, M., Orlandini, E., Osborn, W., Yeomans, J., 1996. Lattice Boltzmann simulations of liquid–gas and binary fluid systems. Phys. Rev. E 54, 5041–5052.
Ubertini, S., Bella, G., Succi, S., 2003. Lattice boltzmann method on unstructured grids: further developments. Phys. Rev. E 68, 016701.
Wang, X., Xu, X., Choi, U.S., 1999. Thermal conductivity of nanoparticle fluid mixture. J. Thermophys. Heat Transfer 13, 474–480.
Wen, D., Ding, Y., 2004. Experimental investigation into convective heat transfer of nanofluids at the entrance region under laminar flow conditions. Int. J. Heat Mass Transfer 47, 5181–5188.
Xuan, Y., Li, Q., 2000. Heat transfer enhancement of nano-fluids. Int. J. Heat Fluid Flow 21, 58–64.
Xuan, Y., Yao, Z., 2005. Lattice Boltzmann modal for nanofluids. Heat Mass Transfer 41, 199–205.
Xuan, Y., Li, Q., Ye, M., 2006. Lattice Boltzmann simulation of flow and heat transfer of ferrofluid. J. Eng. Thermophys. 27, 1020–1022.
Yu, D., Mei, R., Shyy, W., 2002. A multi-block lattice Boltzmann method for viscous fluid flows. Int. J. Numer. Methods Fluids 39, 99–120.